Inverse bubbles from broken supersymmetry

Giulio Barni, 1,* Simone Blasi, 2,† and Miguel Vanvlasselaer, and Miguel Vanvlasselaer ¹Instituto de Física Teórica IFT-UAM/CSIC, Cantoblanco, E-28049, Madrid, Spain ²Deutsches Elektronen-Synchrotron DESY, Notkestraße 85, 22607 Hamburg, Germany ³Theoretische Natuurkunde and IIHE/ELEM, Vrije Universiteit Brussel, and The International Solvay Institutes, Pleinlaan 2, B-1050 Brussels, Belgium

(Received 17 March 2025; revised 11 June 2025; accepted 15 October 2025; published 7 November 2025)

Building upon the recent findings regarding inverse phase transitions in the early Universe, we present the first natural realization of this phenomenon within a supersymmetry-breaking sector. We demonstrate that inverse hydrodynamics, which is characterized by the fluid being sucked by the bubble wall rather than being pushed or dragged, is actually not limited to a phase of (re)heating but can also occur within the standard cooling cosmology. Through a numerical analysis of the phase transition, we establish a simple and generic criterion to determine its hydrodynamics based on the generalized pseudotrace. Our results provide a proof of principle highlighting the need to account for these new fluid solutions when considering cosmological phase transitions and their phenomenological implications.

DOI: 10.1103/pmf7-vlvc

I. INTRODUCTION

Phase transitions (PTs) in the early Universe plasma, usually called "cosmological" phase transitions, are fascinating phenomena. First-order PTs (FOPTs) proceeding via the nucleation and expansion of bubbles of the true vacuum inside a sea of false vacuum are of particular interest as they can be at the origin of the matter-antimatter asymmetry of the Universe (baryogenesis) [1–14], lead to the production of dark matter [15–27] and primordial black holes [28–32], and can be a powerful source of primordial gravitational waves (GWs) as well [33-37]. The broad program to discover and investigate a possible background of GWs by current experiments such as LIGO-Virgo-KAGRA [38] and pulsar timing arrays [39], as well as future detectors such as the Laser Interferometer Space Antenna [40] and the Einstein Telescope [41], opens the unique opportunity of probing the existence of FOPTs and of new fundamental physics. Indeed, FOPTs appear naturally in a large variety of scenarios beyond the Standard Model (BSM) like composite Higgs [42–46], extended Higgs sectors [47–54], axion models [55,56], dark Yang-Mills sectors [57,58], B - L-breaking sectors

Contact author: giulio.barni@ift.csic.es Contact author: simone.blasi@desy.de *Contact author: miguel.vanvlasselaer@vub.be

Published by the American Physical Society under the terms of the Creative Commons Attribution 4.0 International license. Further distribution of this work must maintain attribution to the author(s) and the published article's title, journal citation, and DOI. Funded by SCOAP³.

[59,60], and supersymmetry- (SUSY) breaking sectors [61,62] and may also be catalyzed by impurities in the early Universe, see, e.g., [63-75], as well as occur in the late Universe in the core of neutron stars [69,76–78].

The dynamics of FOPTs involve a nontrivial interplay between the bubble wall and the surrounding plasma, which is pivotal in determining the phenomenology of the PT including the GW emission. The hydrodynamical modes describing the bulk fluid motion in the background of an expanding bubble during a direct FOPT have been classified a long time ago [79-82]: they consist of detonations, hybrids, and deflagrations. For all these solutions, the fluid is either dragged or pushed (or both) by the bubble wall. The bulk fluid velocity is then always aligned with the wall velocity in the plasma frame [83]. In the case of the inverse PTs, the plasma is instead sucked inside the expanding bubble and the fluid flows in the opposite direction of the bubble wall motion [84,85] (see also Ref. [86] for the case of droplet collapse). These solutions have been so far studied in the context of a (re)heating PT [84,85,87], where the temperature of the system increases with time, and thus have been associated with superheated bubbles, see also [88,89].

In this paper, we show that inverse hydrodynamics is actually not limited to the heating scenario mentioned above, but can instead take place during the standard cooling of the Universe as well. Remarkably, we find the emergence of this novel hydrodynamics during a seemingly standard, symmetry-breaking phase transition. This takes place within the context of dynamical SUSY and R symmetry breaking, which represents the first explicit example for this class of FOPTs. Our findings extend the current understanding of what types of cosmological phase transitions can actually take place, thus opening up new directions for studying the corresponding GW signatures and other phenomenological aspects.

II. PTS IN A SUSY-BREAKING SECTOR

Supersymmetry is not a symmetry of the low-energy theory. Therefore, if it is realized at high-energy scales, it must be broken by a dedicated SUSY-breaking sector. A broad class of perturbative SUSY-breaking mechanisms can be described within the framework of an effective field theory that encapsulates the dynamics of the so-called "pseudomodulus." This pseudomodulus corresponds to the scalar component x of the chiral superfield X, which is directly related to SUSY breaking

$$X = \frac{x}{\sqrt{2}}e^{2ia/f_a} + \sqrt{2}\theta\tilde{G} + \theta^2 F,\tag{1}$$

where we have used the standard superspace notation. In our study, as a minimal benchmark model, we focus on the O'Raifeartaigh model [90]. In addition to the pseudomodulus, the SUSY-breaking sector contains four chiral superfields $\phi_1, \tilde{\phi}_1, \phi_2, \tilde{\phi}_2$. The superpotential takes the form

$$W = -FX + \lambda X \phi_1 \tilde{\phi}_2 + m(\phi_1 \tilde{\phi}_1 + \phi_2 \tilde{\phi}_2). \tag{2}$$

The model preserves a global U(1) R symmetry, which typically accompanies dynamical SUSY breaking [91,92] and under which X has charge two, R[X]=2. The vacuum expectation value (VEV) of x is the order parameter for spontaneous R symmetry breaking, while the additional scalar fields from ϕ_i and $\tilde{\phi}_i$ will have vanishing VEV in all phases. The tree-level vacuum energy is $V_{\text{tree}}^{\min} = |F|^2$ with x being a flat direction, indicating that supersymmetry is broken irrespective of $\langle x \rangle$ while R symmetry is preserved only at the origin, $\langle x \rangle = 0$.

The pseudomodulus flat direction is, however, lifted at the loop level, and the shape of the potential for x is controlled by the mass spectrum of the theory. One can see that this includes massive particles from the ϕ_i and $\tilde{\phi}_i$ superfields, with the scalar eigenstates split in pairs around the fermion ones, as well as massless fields from the superfield X corresponding to the pseudomodulus x, the R axion a, and the Goldstino \tilde{G} . At one loop, the potential for x acquires a global minimum at the origin, while remaining remarkably flat at large field values as a reflection of the underlying SUSY.

Finite-temperature effects, on the other hand, break SUSY explicitly and have a strong impact on the pseudo-modulus effective potential. The typical thermal history of the minimal O'Raifeartaigh model considered here is then as follows [62,93,94]: at very high temperatures, $T \gtrsim \sqrt{F}$,

the system has a single vacuum state, $\langle x \rangle = 0$, and R symmetry is preserved. At lower temperatures, a new local minimum of the effective potential appears at relatively large field values, $\langle x \rangle / \sqrt{F} \gg 1$, which becomes the true vacuum of the theory below a certain critical temperature T_c . This vacuum with broken R symmetry will, however, become metastable and eventually disappear at even lower temperatures, given that the only minimum at zero temperature is at $\langle x \rangle = 0$.

Overall, the system undergoes two phase transitions, namely, (1) the breaking of the R symmetry at high temperatures and (2) its restoration at low temperatures, which turn out to be first order and governed by a thermal barrier. More details on the standard derivation of the effective potential for x and the associated thermal history can be found in Supplemental Material, Sec. I [95] and references therein [96–98], as well as in Ref. [62].

In this paper, we will focus on the first transition that will take place in the expanding Universe, namely, the R symmetry-breaking FOPT: $\langle x=0 \rangle \rightarrow \langle x \neq 0 \rangle$. As it turns out, this FOPT can actually proceed according to either the direct or the inverse hydrodynamics (the latter presented in Refs. [84,85]) depending on the microscopic coupling constant λ entering the superpotential in Eq. (2), while the second R symmetry-restoring FOPT will always be direct.

III. THERMODYNAMICS AND HYDRODYNAMICS OF R SYMMETRY BREAKING

In the early Universe, FOPTs can be modeled as the interplay between a scalar field ϕ , whose vacuum expectation value represents the order parameter of the transition, and the surrounding plasma, which is often well described by a relativistic fluid. The energy-momentum tensor of the system consists then of those two contributions, $T^{\mu\nu} = T^{\mu\nu}_{\rm fluid} + T^{\mu\nu}_{\phi}$, with

$$T^{\mu\nu}_{\phi} = \partial^{\mu}\phi\partial^{\nu}\phi - g^{\mu\nu}\left(\frac{1}{2}(\partial\phi)^2 - V(\phi)\right), \quad (3a)$$

$$T_{\text{fluid}}^{\mu\nu} = (e+p)u^{\mu}u^{\nu} - pg^{\mu\nu}, \tag{3b}$$

where u^{μ} is the four-velocity of the fluid, e is the energy density, p is the pressure, and $V(\phi)$ is the scalar potential. The pressure is related to the free energy as $p=-\mathcal{F}$, while the energy and enthalpy density are given by

$$e = T\frac{dp}{dT} - p,$$
 $w = e + p = T\frac{dp}{dT}.$ (4)

In any particle physics model that can be solved (even if only approximately, e.g., in a loop expansion), the free energy \mathcal{F} can be obtained directly from the effective potential at finite temperature, $V_0 + V_T \equiv \mathcal{F}$. Consequently, the knowledge of the free energy of a given

theory allows us to compute all the thermodynamic quantities of interest without introducing a simplified equation of state (EOS) for the fluid, such as, for instance, the bag EOS and its generalizations.

The conservation of the energy-momentum tensor across the phase boundary, $\nabla_{\mu}T^{\mu\nu}=0$, gives the following relations between the velocities, the energies, and the pressures [99]:

$$v_{+}v_{-} = \frac{p_{+} - p_{-}}{e_{+} - e_{-}}, \qquad \frac{v_{+}}{v_{-}} = \frac{e_{-} + p_{+}}{e_{+} + p_{-}},$$
 (5)

where the subscript "±" denotes quantities in front of/behind the phase boundary, so that, for instance, "-" always represents the interior of the bubble.

We defined inverse PTs as transitions displaying negative bulk velocities in the plasma frame: rather than being pushed outward, the surrounding plasma is drawn inward, effectively being sucked into the expanding bubble. Let us now provide a sharper characterization, or criterion, of inverse hydrodynamics which extends the intuitive one put forward in Ref. [84], according to which inverse PTs are found when the transition proceeds against the vacuum energy (namely, the T=0 effective potential for the order parameter). We find that a fully general characterization of inverse hydrodynamics can be obtained by defining a generalized pseudotrace α_{θ} , which indicates the strength of the phase transition and extends the definition within the bag EOS adopted in [84] as well as the pseudotrace α_{θ} , introduced in [100],

$$\alpha_{\theta} = \frac{4D\theta}{3w_{+}(T_{+})} = \frac{4\left(De(T_{+}) - \frac{\delta e}{\delta p}(T_{+}, T_{-})Dp(T_{+})\right)}{3w_{+}(T_{+})}, \quad (6)$$

where the D and δ are defined as $Df = f_+(T_+) - f_-(T_+)$ and $\delta f = f_-(T_+) - f_-(T_-)$. For given values of T_\pm , they can be related to v_\pm via the matching conditions in (5), then, inverse hydrodynamics takes place for $\alpha_\theta < 0$, while the standard one is realized for $\alpha_\theta > 0$. In this way, we discover that PTs proceeding against the vacuum energy can none-theless display direct hydrodynamics.

Notice that for relatively weak PTs with $T_+ \simeq T_-$, $\delta e/\delta p \simeq 1/c_{s,-}^2$, with $c_{s,-}$ being the speed of sound in the broken phase, Eq. (6) reduces to α_{θ} as defined in Ref. [100]. In the special case of a strictly constant speed of sound, one can refer to the template $\mu\nu$ model as introduced in Ref. [101] to capture deviations from the relativistic fluid with $c_s^2 \neq 1/3$. In this case, our definition further reduces to α_{θ} as derived within this template. Finally, when the speed of sound is $c_s^2 = 1/3$ as for a relativistic gas, this definition reduces to α_+ as considered in Ref. [84].

One can show that FOPTs with $\alpha_{\theta} = 0$ represent the limit of weak hydrodynamics, where $\Delta e = 0$ and $\Delta p = 0$,

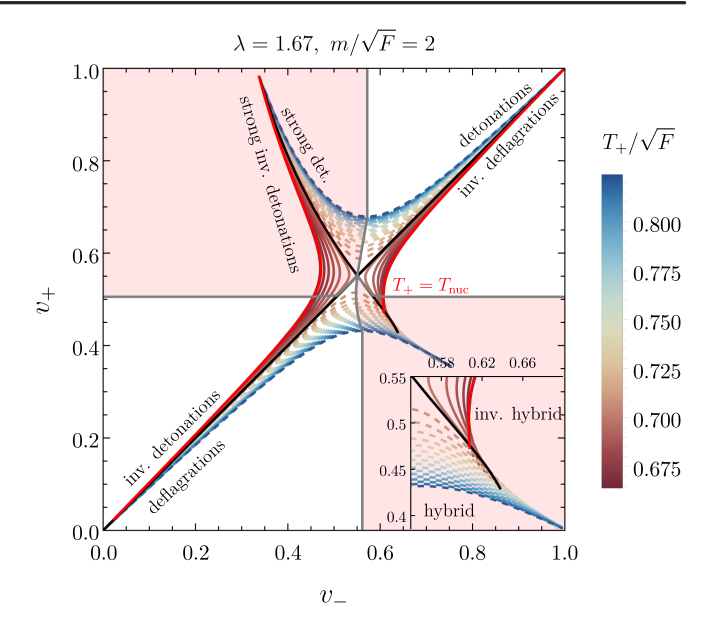


FIG. 1. Possible solutions to the fluid matching conditions for (v_-,v_+) for the R symmetry-breaking FOPT under consideration, plotting the relevant branches for different values of T_+ between T_c and the temperature where the barrier disappears. Dashed lines correspond to direct phase transitions, while solid lines indicate inverse transitions, as determined by the sign of α_{θ} . The solid red line highlights the relevant branch at $T_{\rm nuc}$. The redshaded area marks the region of strong (inverse) detonations and strong (inverse) deflagrations. In the bottom right corner, an enlarged view of the hybrid solution region reveals an overlap between different branches (see Appendix B for more details).

with $\Delta f = f_+(T_+) - f_-(T_-)$. By continuity, this is supposed to separate inverse from direct FOPTs.

Let us now examine the possible hydrodynamics of the R symmetry-breaking FOPT. The junction conditions above can be solved numerically by referring to the pressure and energy densities as evaluated directly from the free energy within our particle physics model. The allowed values for the (v_-, v_+) pairs are shown in Fig. 1 for a representative benchmark point. The matching conditions in Eq. (5) are solved for v_+ in terms of the temperatures ahead and behind the wall, T_{\pm} . For consistency, we restrict T_{+} to lie between T_c and the temperature when the barrier disappears, as this is the range for which the FOPT can actually take place. The various v_+ trajectories in Fig. 1 are then shown together with the corresponding temperature T_{+} according to the color code. Because of the consistency condition on T_{+} and the properties of our system free energy, the branches do not populate the entire $v_{\pm} \in (0, 1)$ parameter space. The regions corresponding to inverse and direct hydrodynamics, according to the sign of α_{θ} , are indicated by solid and dashed lines, respectively. We find that these regions remain neatly separated across the entire (v_-, v_+) plane, except for a small overlap in the regime of hybrid solutions (bottom right corner). As a comparison, a similar discussion of the inverse branches in the case of the simplified (template) $\mu\nu$ model is

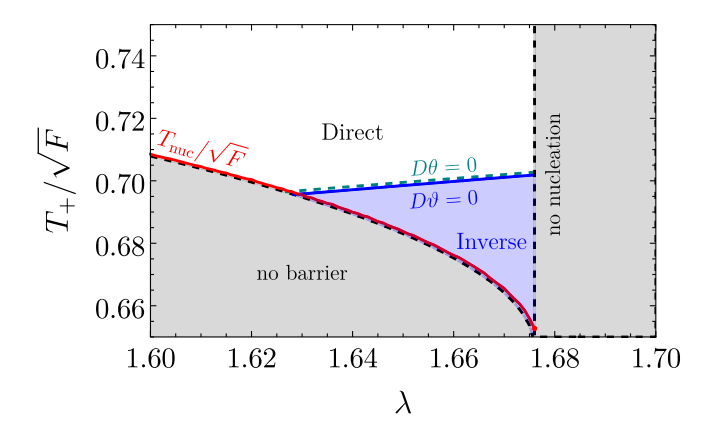


FIG. 2. The nucleation temperature (red line) is obtained as a function of λ by numerically solving the condition $S_3/T=140$, which corresponds to setting $\sqrt{F} \sim \text{TeV}$ for concreteness (see Supplemental Material, Sec. II [95]). The blue-shaded (white) region indicates the occurrence of the inverse (direct) FOPTs, whose boundary is shown according to the criteria $D\theta=0$ and $D\theta=0$. For this figure, we fixed $m/\sqrt{F}=2$.

provided in Appendix A, where we find qualitative agreement with the full numerical study of the SUSY model presented here.

In the early Universe, bubbles are efficiently formed when the nucleation rate catches up with the Hubble expansion. This condition, presented in more detail in Supplemental Material, Sec. II [95] and Refs. [102–107], connects the onset of the FOPT with a certain nucleation temperature $T_{\rm nuc}$. If we then further specify the temperature of the FOPT as $T_{\rm nuc}$ [108], we can select the bright red branch as the relevant one for this specific benchmark point. Notice that, as the matching conditions cannot uniquely determine the bubble wall velocity, the actual value of v_{+} cannot be pinned down by the hydrodynamics only, and the full red branch can, in principle, be realized. On the other hand, when taking the wall velocity as an additional input, the fluid profile can be fully determined. As we can see, the FOPT within this benchmark point occurs in the inverse hydrodynamic regime.

In Fig. 2, we perform a scan over the model parameter space, by fixing $m/\sqrt{F}=2$ and varying the coupling constant λ . The red line indicates the nucleation temperature, which always happens to be very close to the temperature where the barrier actually disappears. For $\lambda \lesssim 1.63$, bubble nucleation occurs in the region where the hydrodynamics will be the one based on the (direct) detonation and deflagration types of solutions, while for $1.63 \lesssim \lambda \lesssim 1.68$ the hydrodynamics will be inverse. We can also notice that the condition of vanishing α_{θ} actually corresponds to the boundary between direct and inverse regions, which are determined independently by solving the fluid equations. As we can see, the approximate condition in terms of the pseudotrace, $\alpha_{\theta}=0$, reproduces this separation fairly well. This can be traced back to the fact that the speed

of sound is not strongly temperature dependent in this model.

IV. INVERSE FLUID SOLUTIONS FOR R SYMMETRY BREAKING

The hydrodynamics of inverse PTs was presented for the first time in Refs. [84,85] (see also [109]). There exist five different possible expansion modes with negative bulk velocities: (i) inverse detonations [weak and Chapman-Jouguet (CJ)], (ii) inverse deflagrations (weak and CJ), and (iii) inverse hybrids.

This classification of hydrodynamic solutions was obtained within the (simplified) bag EOS. We have checked that this picture remains qualitatively the same also when considering the full form of the free energy (or effective potential) as evaluated explicitly for the SUSY model under consideration. In practice, we find only some quantitative differences related to the actual value of the speed of sound, which generally differs from $c_s^2 = 1/3$, and to the (mild) temperature dependence of c_s^2 , which requires solving the coupled system of fluid equations for the pressure and the energy density as discussed in Appendix B. An example of the explicit profiles obtained by solving numerically the fluid equations for the benchmark point with $\lambda = 1.67$ and $m/\sqrt{F} = 2$ is shown in detail in Fig. 3 for an inverse detonation, together with the free energy of the system at the nucleation temperature showing the direction of the phase transition and a sketch of the bubble with the corresponding fluid profile.

Let us also mention that there is, in principle, the possibility that the bubble wall never reaches any of the steady states presented above and keeps accelerating until bubbles collide, namely, it runs away. Employing the line of reasoning presented in Ref. [84], we find that the bubble never runs away in the model under consideration and always reaches one of the steady states (see Supplemental Material, Sec. III [95] and Refs. [110–112] for a derivation). Our hydrodynamic analysis, however, cannot determine which one of them, as mentioned above.

V. COUPLING TO THE STANDARD MODEL THERMAL BATH

In the early Universe, the SUSY-breaking sector considered here is generally accompanied by additional spectator fields [113] that are in thermal equilibrium with the SUSY-breaking sector and constitute a radiation bath. To assess the impact of these additional degrees of freedom, we redefine the energy and pressure as

$$p(T) \rightarrow p(T) + \tilde{c}^2 \tilde{a} T^4, \quad e(T) \rightarrow e(T) + 3\tilde{c}^2 \tilde{a} T^4, \quad (7)$$

where $\tilde{c}^2 = 1/3$, and \tilde{a} controls the number of the relativistic spectator degrees of freedom (d.o.f.), which is

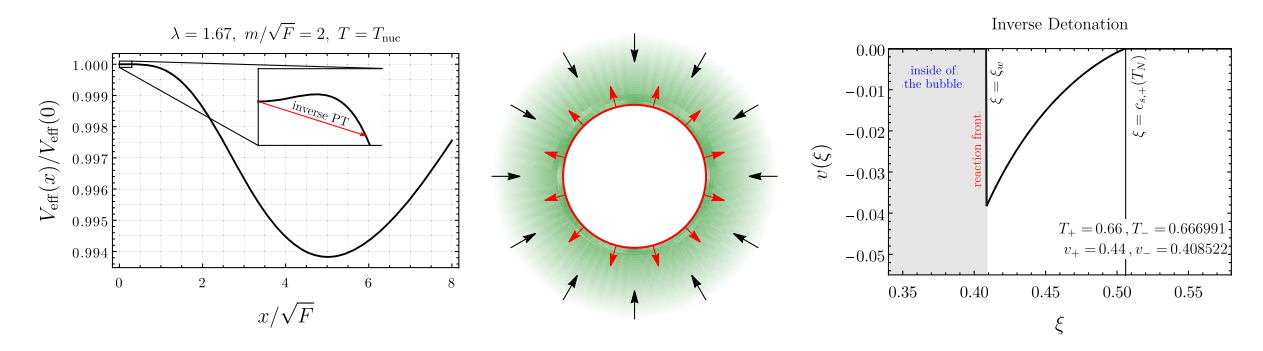


FIG. 3. Free energy of the system at finite temperature evaluated at one loop at the nucleation temperature, with the arrow indicating the direction of the phase transition toward the minimum with a nonzero x (left), together with a sketch of the expanding bubble and its velocity in red and the fluid profile in green (center) for a characteristic inverse detonation. The actual fluid profile in the plasma frame is shown on the right. Because of its inverse nature, the fluid velocity is always negative. See main text and Appendix B for details.

expected to be $\tilde{a} \sim 70$ considering a supersymmetric extension of the Standard Model.

The presence of these fields will mostly influence the strength of the FOPT. In the limit $\tilde{a} \gg 1$, one has $\delta p/\delta e \simeq 1/3$ as expected for a gas of relativistic particles, and the generalized pseudotrace in this limit becomes

$$\alpha_{\vartheta} \simeq \frac{4(De - 3Dp)}{3w_{+}(T_{+})} \frac{1}{1+x}, \qquad x = \frac{4\tilde{c}^{2}\tilde{a}T_{+}^{4}}{w_{+}(T_{+})}.$$
 (8)

Thus, to a good approximation, the strength of the phase transition exhibits an inverse scaling with \tilde{a} , aligning with physical intuition. From explicit calculations, we find that the pseudotrace and generalized pseudotrace are always very close to each other in the parameter space of interest, and that the asymptotic behavior in Eq. (8) is well established for $\tilde{a} \gtrsim 50$, leading to typical values of $\alpha_{\theta} \lesssim 10^{-2}$, while in the absence of spectator fields, one would have $\alpha_{\theta} \lesssim 10^{-1}$.

In this regard, let us notice that there is, in fact, a fundamental difference between the strength of a standard (direct) FOPT and the case of an inverse FOPT. By referring to the definition of α_{θ} in Eq. (6), we can see that the part containing $Dp(T_+)$ will always contribute with a positive sign. This follows from the fact that the broken phase will necessarily have a larger pressure than the symmetric phase for the FOPT to take place and that $\delta e/\delta p \simeq 1/c_s^2$ is a positive quantity. Therefore, considering the case of negative α_{θ} , we can derive the following inequality:

$$\frac{3}{4}|\alpha_{\theta}| < \frac{w_{-}(T_{+}) - w_{+}(T_{+})}{w_{+}(T_{+})} = \frac{\Delta a_{\text{eff}}(T_{+})}{a_{\text{eff},+}(T_{+})}, \quad (9)$$

where $a_{\rm eff,+}(T_+)$ indicates the effective number of relativistic d.o.f. in the symmetric phase at the temperature T_+ , according to the parametrization $3w(T)/4T^4 \equiv a_{\rm eff}(T)$, and $\Delta a_{\rm eff}(T_+)$ is the change in d.o.f. in the broken phase at the same temperature. This relation shows that an inverse FOPT can be strong only when it involves a significant change in d.o.f. between the two phases. This is a structural

property of the vacua of the theory under consideration, and it should be contrasted with the case of standard FOPTs whose strength is mostly controlled by the amount of supercooling that can be achieved in the expanding Universe. In particular, Eq. (9) indicates that an inverse FOPT is not necessarily stronger when it becomes more supercooled.

VI. CONCLUSION AND OUTLOOK

We presented a simple SUSY-breaking model displaying a window of inverse FOPTs during the spontaneous breaking of the *R* symmetry. This represents the first explicit example of a BSM model leading to an inverse FOPT in a cooling cosmology, as well as a proof of principle for the relevance of this dynamics in the early Universe.

We find that the sign of the generalized pseudotrace, α_{θ} in Eq. (6), determines the "inverseness" of the transition. As a comparison, we also show that the sign of the pseudotrace introduced in Ref. [100] offers a fair estimate for the type of the FOPT as well.

Our study motivates a broader investigation of inverse FOPTs in explicit BSM models. This includes establishing a deeper connection between the inverseness of a FOPT and its fundamental properties and symmetries, exemplified here within a model of spontaneous SUSY breaking, as well as identifying possible non-SUSY realizations of this dynamics.

Finally, FOPTs are powerful sources of gravitational waves that can be detected at current and forthcoming GW observatories. This work provides motivation to characterize the GW spectrum related to inverse FOPTs and to determine to which extent this can be distinguished from the one arising during direct FOPTs.

ACKNOWLEDGMENTS

We sincerely acknowledge Thomas Konstandin, Xander Nagels, Alberto Mariotti, David Mateos, Diego Redigolo,

and Mikel Sanchez-Garitaonandia for clarifying discussions and for reading the manuscript. G. B. is supported by the Grant No. CNS2023-145069 funded by MICIU/AEI/10.13039/501100011033 and by the European Union NextGenerationEU/PRTR. G. B. also acknowledges the support of the Spanish Agencia Estatal de Investigacion through the Grant "IFT Centro de Excelencia Severo Ochoa CEX2020-001007-S". S. B. is supported by the Deutsche Forschungsgemeinschaft under Germany's Excellence Strategy—EXC 2121 Quantum Universe—390833306. M. V. is supported by the "Excellence of Science—EOS"—be.h Project No. 30820817 and by the Strategic Research Program High-Energy Physics of the Vrije Universiteit Brussel.

DATA AVAILABILITY

The data are not publicly available. The data are available from the authors upon reasonable request.

APPENDIX A: INVERSE FOPTS IN THE $\mu\nu$ MODEL

In this appendix, we examine the emergence of inverse phase transitions in the $\mu\nu$ model [101], also referred to as the ν model in Ref. [100] and the template model in Refs. [110,114,115]. The $\mu\nu$ model extends the standard bag model by allowing the sound speed to deviate from the relativistic value of $1/\sqrt{3}$, while remaining constant within each phase. Explicitly, the EOS for the symmetric and broken phases is given by

$$e_{\pm}(T) = a_{\pm}T^{\nu_{\pm}} + \epsilon_{\pm}, \qquad p_{\pm}(T) = c_{s,+}^2 a_{\pm}T^{\nu_{\pm}} - \epsilon_{\pm},$$
 (A1)

In the following $\nu_+ \equiv \nu$ and $\nu_- \equiv \mu$, we consider $\mu > \nu$ as this mimics the thermal history of the *R* symmetry model, presented in the main text. The velocity relations from the matching conditions take the form

$$\begin{split} v_{+}v_{-} &= \frac{\mu - \mu\nu - r\nu(3\alpha_{\theta} - 1)(\mu - 1)}{(\mu - \mu\nu + r\nu(3\alpha_{\theta} + \mu - 1))(\mu - 1)}, \\ \frac{v_{+}}{v_{-}} &= \frac{(\mu - 1)(\mu - \mu\nu + r\nu(3\alpha_{\theta} - 1))}{\mu - \mu\nu - r\nu(3\alpha_{\theta} + \mu - 1)(\mu - 1)}, \end{split} \tag{A2a}$$

where we define the ratio $r \equiv a_+ T_+^{\nu}/a_- T_-^{\mu}$. Additionally, the strength parameter α_{θ} , defined from the pseudotrace θ as $\alpha_{\theta} \equiv 4D\theta/3w_+$ where $\theta = e - p/c_{s,-}^2$, within the $\mu\nu$ model evaluates to

$$\alpha_{\theta} = \frac{\nu - 1}{3\nu} \left(\frac{\nu - \mu}{\nu - 1} + \mu \alpha_{+} \right), \quad \alpha_{+} \equiv \frac{\Delta \epsilon}{a_{+} T_{+}^{\nu}} = \frac{\epsilon_{+} - \epsilon_{-}}{a_{+} T_{+}^{\nu}}. \quad (A3)$$

It is important to emphasize that α_{θ} serves as the fundamental quantity determining the nature of the transition and

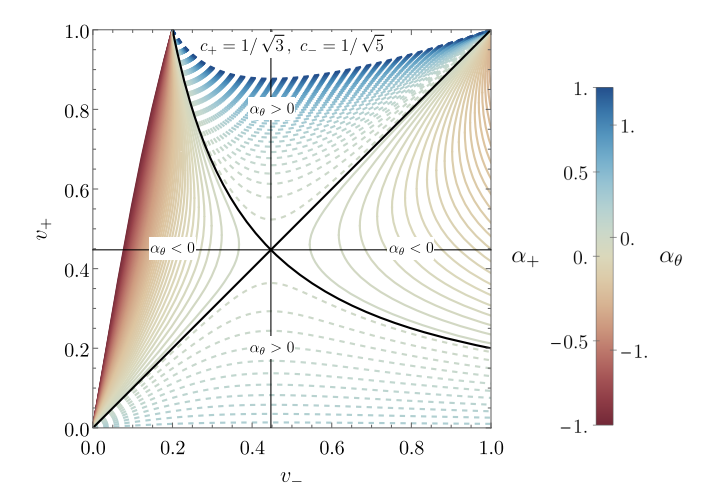


FIG. 4. Dashed (solid) lines represent direct (inverse) phase transitions. The inverse branches emerge as soon as $\alpha_{\theta} < 0$, whereas this is not necessarily the case for α_{+} . The two strength parameters of the phase transition, α_{+} and α_{θ} , coincide in the bag model when $\mu = \nu = 4$.

directly corresponds to the strength of the phase transition computed via the pseudotrace.

Notably, in the case of the traditional bag EOS, where $\mu = \nu = 4$, the pseudotrace coincides with the standard definition of the phase transition strength, $\alpha_{\theta} = \alpha_{+}$, thereby recovering the standard velocity relations.

It is shown in Fig. 4 that, as soon as $\alpha_{\theta} < 0$, the "inverse branches" emerge. This confirms that, in the $\mu\nu$ model, a negative α_{θ} implies an inverse phase transition. Analogously, for the bag EOS, a negative α_{+} corresponds to an inverse PT. This result aligns with the characterization proposed in [84], where it was shown that, within the bag EOS, $\Delta \epsilon < 0$ serves as a direct indicator of an inverse phase transition.

APPENDIX B: SOLVING THE HYDRODYNAMIC EQUATIONS FOR THE FLUID PROFILES

The conservation of the energy-momentum tensor for a relativistic fluid, given by $\nabla_{\mu}T^{\mu\nu}=0$, yields two independent hydrodynamic equations. These equations can be rewritten in terms of the enthalpy density, w=e+p. We consider a spherically symmetric and self-similar configuration, where the fluid variables depend only on $\xi\equiv r/t$, the similarity variable. Using this variable, it can be shown that the hydrodynamics equations, in terms of the fluid velocity $v(\xi)$ and the fluid temperature $T(\xi)$, take the following form:

$$(\xi - v) \frac{\partial_{\xi} T}{w} \frac{de}{dT} = \frac{2v}{\xi} + [1 - \gamma^2 v(\xi - v)] \partial_{\xi} v,$$

$$\frac{\partial_{\xi} T}{T} = \gamma^2 \mu(\xi, v) \partial_{\xi} v,$$
(B1)

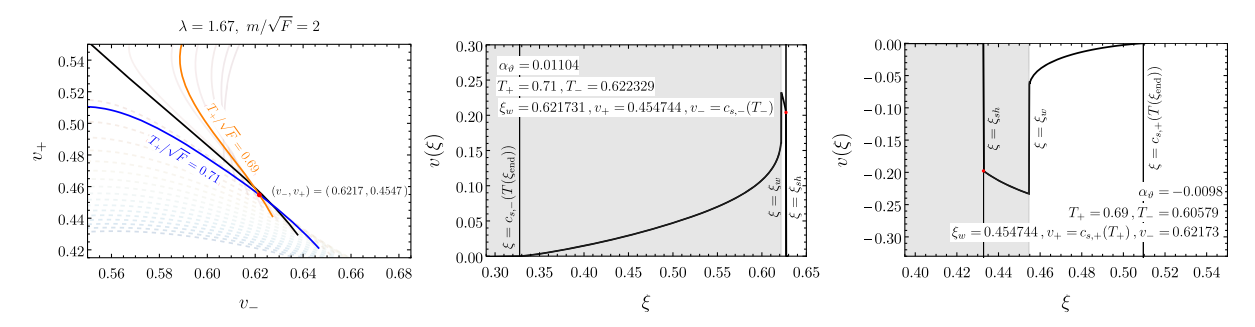


FIG. 5. Overlap of direct and inverse branches in the (v_-, v_+) plane and corresponding fluid profiles. Left: the (v_-, v_+) trajectories for different values of T_+ . The inverse branch is shown in orange, while the direct branch is displayed in blue. The highlighted crossing point indicates a case where both a direct and an inverse solution exist for the same (v_-, v_+) pair. Middle: fluid profile corresponding to the direct hybrid solution. Right: fluid profile for the inverse hybrid solution. The shaded regions indicate the interior of the bubble.

where $\mu(\xi, v) = \frac{\xi - v}{1 - \xi v}$. It is important to emphasize that the thermodynamic quantities, such as p and e, must be evaluated in the appropriate phase depending on the region where the equation is being solved. In the remainder of this appendix, we present the different types of expansion modes for inverse PTs within this general framework.

1. Inverse deflagration

To fully specify the system of equations in Eq. (B1), we must define the initial conditions for $v(\xi)$ and $T(\xi)$. In the case of an inverse deflagration, this translates to

$$\begin{split} \xi_w &= v_+, & v(\xi_w) = \mu(v_+, v_-), \\ T(\xi_w^+) &= T_+, & T(\xi_w^-) = T_-, \end{split} \tag{B2}$$

where the + phase corresponds to the false vacuum, while the – phase corresponds to the true vacuum. Additionally, we impose the condition for the formation of a shock wave, which is given by $\mu(\xi_{sh}, v(\xi_{sh}))\xi_{sh} = c_{s,-}^2(T(\xi_{sh}))$. These initial conditions also apply to standard detonations, provided that the pair (v_+, v_-) satisfies the condition $v_+ > v_-$.

2. Inverse detonations

For inverse detonations, the initial conditions across the discontinuity translate into

$$\begin{split} \xi_w &= v_-, & v(\xi_w) &= \mu(v_-, v_+), \\ T(\xi_w^+) &= T_+, & T(\xi_w^-) &= T_-. \end{split} \tag{B3}$$

It can be checked directly that the rarefaction wave terminates at $\xi_{\rm end} = c_{s,+}(T(\xi_{\rm end}))$. For a standard detonation, the substitution $c_{s,+} \to c_{s,-}$ must be applied, as the rarefaction wave develops behind the reaction front, i.e., in the new phase.

These initial conditions also apply to standard deflagrations, provided that the pair (v_+,v_-) satisfies the appropriate conditions. In this case, the shock condition must be

modified by replacing $c_{s,-}$ with $c_{s,+}$, as the shock forms ahead of the reaction front in the old phase.

Before discussing the last type of solution, it is important to highlight the presence of strong solutions in Fig. 5, where the red-shaded region indicates their domain. For (inverse) detonations/deflagrations, the strong regime is defined by the conditions $(v_+ \geq c_{s,+}(T_+))v_- \leq c_{s,-}(T_-)$. As previously discussed in [84], strong (inverse) detonations cannot be consistently realized, while strong (inverse) deflagrations, although they may initially form due to the dynamics of the phase transition, are inherently unstable. Over time, they will decay into (inverse) hybrid solutions.

3. Inverse hybrid

For inverse hybrid solutions, as in the standard case, to make the profile stable, we must connect a strong inverse deflagration to a Chapman-Jouguet inverse detonation, which is defined as a detonation with $v_+ = c_{s,+}(T_+)$. The initial conditions then translate into

$$\begin{split} v(\xi_w^+) &= \mu(\xi_w^+, c_{s,+}(T_+)), \qquad v(\xi_w^-) = \mu(\xi_w^-, v_-), \\ T(\xi_w^+) &= T_+, \qquad T(\xi_w^-) = T_-, \end{split} \tag{B4}$$

where the four input parameters required to specify the system are (ξ_w, v_-, T_+, T_-) .

Additionally, the shock formation condition must be imposed, and one can verify that the rarefaction wave of the inverse detonation terminates again at $\xi_{\rm end} = c_{s,+}(T(\xi_{\rm end}))$. The maximal range of wall velocities for which an inverse hybrid solution exists is given by $c_{s,-}^2 < \xi_w < c_{s,+}$, where the lower bound arises because the slowest possible inverse hybrid is determined by the slowest possible shock.

For the case of a direct hybrid transition, a strong deflagration must instead be connected to a CJ detonation, where the latter is characterized by $v_- = c_{s,-}(T_-)$. The allowed range of wall velocities in this case is $c_{s,-} < \xi_w < 1$ where the upper bound is simply the speed of light, as there is no fundamental constraint on the maximum speed of the shock front.

4. Overlap in the hybrid corner

In our numerical analysis, we observe that, in the hybrid transition regime, the branches in the (v_-, v_+) plane exhibit an overlap between direct and inverse transitions. This is particularly evident when focusing in on the hybrid region, as shown in Fig. 5 (left panel). There, we explicitly construct two distinct solutions corresponding to the same pair of values (v_-, v_+) , demonstrating the existence of overlapping branches, in the middle and right panels of Fig. 5.

This overlap arises due to the stability conditions required for hybrid solutions. Specifically, for both direct and inverse hybrids to remain stable, the fluid velocity just behind (or in front of) the wall must match the local speed of sound in the respective phase at the corresponding temperature. That is, stability demands that for (inverse) hybrid holds $(v_+ = c_{s,+}(T_+))v_- = c_{s,-}(T_-)$. This condition provides additional flexibility in setting $\xi_w = v_-$ for

direct hybrids and $\xi_w = v_+$ for inverse hybrids, thus allowing both solutions to coexist.

Another key reason for this overlap is related to the structure of the separatrices (black solid lines) in the (v_-, v_+) plane. Ideally, these separatrices would be given by $v_- = v_+$ and $v_-v_+ = c_{s,-}^2$, however, since the speed of sound varies along the branches due to temperature dependence, the boundary between the direct and inverse solutions is no longer sharply defined. Despite their overlap in the (v_-, v_+) plane, the two solutions can still be distinguished physically. Each branch corresponds to a different set of temperatures (T_+, T_-) , leading to a different transition strength characterized by the generalized pseudotrace α_θ , which will have, in fact, a different sign. Thus, even though the solutions may appear degenerate in velocity space, they remain distinct due to their thermodynamic properties.

- [1] V. A. Kuzmin, V. A. Rubakov, and M. E. Shaposhnikov, On the anomalous electroweak baryon number nonconservation in the early Universe, Phys. Lett. **155B**, 36 (1985).
- [2] M. Shaposhnikov, Possible appearance of the baryon asymmetry of the Universe in an electroweak theory, JETP Lett. 44, 465 (1986), https://inspirehep.net/literature/241033.
- [3] A. E. Nelson, D. B. Kaplan, and A. G. Cohen, Why there is something rather than nothing: Matter from weak interactions, Nucl. Phys. **B373**, 453 (1992).
- [4] M. Carena, M. Quiros, and C. E. M. Wagner, Opening the window for electroweak baryogenesis, Phys. Lett. B 380, 81 (1996).
- [5] J. M. Cline, Is electroweak baryogenesis dead?, Phil. Trans. R. Soc. A 376, 20170116 (2018).
- [6] A. J. Long, A. Tesi, and L.-T. Wang, Baryogenesis at a lepton-number-breaking phase transition, J. High Energy Phys. 10 (2017) 095.
- [7] S. Bruggisser, B. Von Harling, O. Matsedonskyi, and G. Servant, Electroweak phase transition and baryogenesis in composite Higgs models, J. High Energy Phys. 12 (2018) 099.
- [8] S. Bruggisser, B. Von Harling, O. Matsedonskyi, and G. Servant, Baryon asymmetry from a composite Higgs boson, Phys. Rev. Lett. 121, 131801 (2018).
- [9] S. Bruggisser, B. von Harling, O. Matsedonskyi, and G. Servant, Status of electroweak baryogenesis in minimal composite Higgs, J. High Energy Phys. 08 (2023) 012.
- [10] D. E. Morrissey and M. J. Ramsey-Musolf, Electroweak baryogenesis, New J. Phys. 14, 125003 (2012).
- [11] A. Azatov, M. Vanvlasselaer, and W. Yin, Baryogenesis via relativistic bubble walls, J. High Energy Phys. 10 (2021) 043.
- [12] P. Huang and K.-P. Xie, Leptogenesis triggered by a first-order phase transition, J. High Energy Phys. 09 (2022) 052.

- [13] I. Baldes, S. Blasi, A. Mariotti, A. Sevrin, and K. Turbang, Baryogenesis via relativistic bubble expansion, Phys. Rev. D 104, 115029 (2021).
- [14] E. J. Chun, T. P. Dutka, T. H. Jung, X. Nagels, and M. Vanvlasselaer, Bubble-assisted leptogenesis, J. High Energy Phys. 09 (2023) 164.
- [15] A. Falkowski and J. M. No, Non-thermal dark matter production from the electroweak phase transition: Multi-TeV WIMPs and 'Baby-Zillas', J. High Energy Phys. 02 (2013) 034.
- [16] I. Baldes, Y. Gouttenoire, and F. Sala, String fragmentation in supercooled confinement and implications for dark matter, J. High Energy Phys. 04 (2021) 278.
- [17] J.-P. Hong, S. Jung, and K.-P. Xie, Fermi-ball dark matter from a first-order phase transition, Phys. Rev. D 102, 075028 (2020).
- [18] A. Azatov, M. Vanvlasselaer, and W. Yin, Dark matter production from relativistic bubble walls, J. High Energy Phys. 03 (2021) 288.
- [19] I. Baldes, Y. Gouttenoire, F. Sala, and G. Servant, Supercool composite dark matter beyond 100 TeV, J. High Energy Phys. 07 (2022) 084.
- [20] P. Asadi, E. D. Kramer, E. Kuflik, G. W. Ridgway, T. R. Slatyer, and J. Smirnov, Thermal squeezeout of dark matter, Phys. Rev. D 104, 095013 (2021).
- [21] P. Lu, K. Kawana, and K.-P. Xie, Old phase remnants in first-order phase transitions, Phys. Rev. D 105, 123503 (2022).
- [22] I. Baldes, Y. Gouttenoire, and F. Sala, Hot and heavy dark matter from a weak scale phase transition, SciPost Phys. 14, 033 (2023).
- [23] A. Azatov, G. Barni, S. Chakraborty, M. Vanvlasselaer, and W. Yin, Ultra-relativistic bubbles from the simplest Higgs portal and their cosmological consequences, J. High Energy Phys. 10 (2022) 017.

- [24] I. Baldes, M. Dichtl, Y. Gouttenoire, and F. Sala, Bubbletrons, Phys. Rev. Lett. 134, 061001 (2025).
- [25] M. Kierkla, A. Karam, and B. Swiezewska, Conformal model for gravitational waves and dark matter: A status update, J. High Energy Phys. 03 (2023) 007.
- [26] G. F. Giudice, H. M. Lee, A. Pomarol, and B. Shakya, Nonthermal heavy dark matter from a first-order phase transition, J. High Energy Phys. 12 (2024) 190.
- [27] A. Azatov, X. Nagels, M. Vanvlasselaer, and W. Yin, Populating secluded dark sector with ultra-relativistic bubbles, J. High Energy Phys. 11 (2024) 129.
- [28] H. Kodama, M. Sasaki, and K. Sato, Abundance of primordial holes produced by cosmological first order phase transition, Prog. Theor. Phys. 68, 1979 (1982).
- [29] K. Kawana and K.-P. Xie, Primordial black holes from a cosmic phase transition: The collapse of Fermi-balls, Phys. Lett. B 824 (2022) 136791,
- [30] T. H. Jung and T. Okui, Primordial black holes from bubble collisions during a first-order phase transition, Phys. Rev. D 110, 115014 (2024).
- [31] Y. Gouttenoire and T. Volansky, Primordial black holes from supercooled phase transitions, Phys. Rev. D 110, 043514 (2024).
- [32] M. Lewicki, P. Toczek, and V. Vaskonen, Primordial black holes from strong first-order phase transitions, J. High Energy Phys. 09 (2023) 092.
- [33] E. Witten, Cosmic separation of phases, Phys. Rev. D 30, 272 (1984).
- [34] C. J. Hogan, Gravitational radiation from cosmological phase transitions, Mon. Not. R. Astron. Soc. 218, 629 (1986).
- [35] A. Kosowsky and M. S. Turner, Gravitational radiation from colliding vacuum bubbles: Envelope approximation to many bubble collisions, Phys. Rev. D 47, 4372 (1993).
- [36] A. Kosowsky, M. S. Turner, and R. Watkins, Gravitational waves from first order cosmological phase transitions, Phys. Rev. Lett. **69**, 2026 (1992).
- [37] M. Kamionkowski, A. Kosowsky, and M. S. Turner, Gravitational radiation from first order phase transitions, Phys. Rev. D 49, 2837 (1994).
- [38] A. Romero, K. Martinovic, T. A. Callister, H.-K. Guo, M. Martínez, M. Sakellariadou, F.-W. Yang, and Y. Zhao, Implications for first-order cosmological phase transitions from the third LIGO-Virgo observing run, Phys. Rev. Lett. 126, 151301 (2021).
- [39] T. Bringmann, P. F. Depta, T. Konstandin, K. Schmidt-Hoberg, and C. Tasillo, Does NANOGrav observe a dark sector phase transition?, J. Cosmol. Astropart. Phys. 11 (2023) 053.
- [40] C. Caprini et al., Science with the space-based interferometer eLISA. II: Gravitational waves from cosmological phase transitions, J. Cosmol. Astropart. Phys. 04 (2016) 001.
- [41] M. Maggiore *et al.* (ET Collaboration), Science case for the Einstein telescope, J. Cosmol. Astropart. Phys. 03 (2020) 050.
- [42] R. Pasechnik, M. Reichert, F. Sannino, and Z.-W. Wang, Gravitational waves from composite dark sectors, J. High Energy Phys. 02 (2024) 159.

- [43] A. Azatov and M. Vanvlasselaer, Phase transitions in perturbative walking dynamics, J. High Energy Phys. 09 (2020) 085.
- [44] M. T. Frandsen, M. Heikinheimo, M. Rosenlyst, M. E. Thing, and K. Tuominen, Gravitational waves from SU (N)/SP(N) composite Higgs models, J. High Energy Phys. 09 (2023) 022.
- [45] M. Reichert and Z.-W. Wang, Gravitational waves from dark composite dynamics, EPJ Web Conf. 274, 08003 (2022)
- [46] K. Fujikura, Y. Nakai, R. Sato, and Y. Wang, Cosmological phase transitions in composite Higgs models, J. High Energy Phys. 09 (2023) 053.
- [47] C. Delaunay, C. Grojean, and J. D. Wells, Dynamics of non-renormalizable electroweak symmetry breaking, J. High Energy Phys. 04 (2008) 029.
- [48] G. Kurup and M. Perelstein, Dynamics of electroweak phase transition in singlet-scalar extension of the standard model, Phys. Rev. D **96**, 015036 (2017).
- [49] B. von Harling and G. Servant, QCD-induced electroweak phase transition, J. High Energy Phys. 01 (2018) 159.
- [50] A. Azatov, D. Barducci, and F. Sgarlata, Gravitational traces of broken gauge symmetries, J. Cosmol. Astropart. Phys. 07 (2020) 027.
- [51] T. Ghosh, H.-K. Guo, T. Han, and H. Liu, Electroweak phase transition with an SU(2) dark sector, J. High Energy Phys. 07 (2021) 045.
- [52] M. Aoki, T. Komatsu, and H. Shibuya, Possibility of a multi-step electroweak phase transition in the two-Higgs doublet models, Prog. Theor. Exp. Phys. **2022**, 063B05 (2022).
- [53] M. Badziak and I. Nalecz, First-order phase transitions in twin Higgs models, J. High Energy Phys. 02 (2023) 185.
- [54] U. Banerjee, S. Chakraborty, S. Prakash, and S. U. Rahaman, The feasibility of ultra-relativistic bubbles in SMEFT, Phys. Rev. D **110**, 055002 (2024).
- [55] L. Delle Rose, G. Panico, M. Redi, and A. Tesi, Gravitational waves from supercool axions, J. High Energy Phys. 04 (2020) 025.
- [56] B. Von Harling, A. Pomarol, O. Pujolàs, and F. Rompineve, Peccei-Quinn phase transition at LIGO, J. High Energy Phys. 04 (2020) 195.
- [57] J. Halverson, C. Long, A. Maiti, B. Nelson, and G. Salinas, Gravitational waves from dark Yang-Mills sectors, J. High Energy Phys. 05 (2021) 154.
- [58] E. Morgante, N. Ramberg, and P. Schwaller, Gravitational waves from dark SU(3) Yang-Mills theory, Phys. Rev. D **107**, 036010 (2023).
- [59] R. Jinno and M. Takimoto, Probing a classically conformal B-L model with gravitational waves, Phys. Rev. D 95, 015020 (2017).
- [60] A. Addazi, A. Marcianò, A. P. Morais, R. Pasechnik, J. a. Viana, and H. Yang, Gravitational echoes of lepton number symmetry breaking with light and ultralight Majorons, J. Cosmol. Astropart. Phys. 09 (2023) 026; 03 (2024) E01.
- [61] N. J. Craig, Gravitational waves from supersymmetry breaking, arXiv:0902.1990.
- [62] N. Craig, N. Levi, A. Mariotti, and D. Redigolo, Ripples in spacetime from broken supersymmetry, J. High Energy Phys. 21 (2020) 184.

- [63] P.J. Steinhardt, Monopole and vortex dissociation and decay of the false vacuum, Nucl. Phys. B190, 583 (1981).
- [64] Y. Hosotani, Impurities in the early Universe, Phys. Rev. D 27, 789 (1983).
- [65] U. A. Yajnik, Phase transition induced by cosmic strings, Phys. Rev. D 34, 1237 (1986).
- [66] K. Mukaida and M. Yamada, False vacuum decay catalyzed by black holes, Phys. Rev. D 96, 103514 (2017).
- [67] D. Canko, I. Gialamas, G. Jelic-Cizmek, A. Riotto, and N. Tetradis, On the catalysis of the electroweak vacuum decay by black holes at high temperature, Eur. Phys. J. C 78, 328 (2018).
- [68] R. Jinno, T. Konstandin, H. Rubira, and J. van de Vis, Effect of density fluctuations on gravitational wave production in first-order phase transitions, J. Cosmol. Astropart. Phys. 12 (2021) 019.
- [69] R. Balkin, J. Serra, K. Springmann, S. Stelzl, and A. Weiler, Density induced vacuum instability, SciPost Phys. 14, 071 (2023).
- [70] P. Agrawal and M. Nee, The boring monopole, SciPost Phys. 13, 049 (2022).
- [71] S. Blasi and A. Mariotti, Domain walls seeding the electroweak phase transition, Phys. Rev. Lett. 129, 261303 (2022).
- [72] P. Agrawal, S. Blasi, A. Mariotti, and M. Nee, Electroweak phase transition with a double well done doubly well, J. High Energy Phys. 06 (2024) 089.
- [73] R. Jinno, J. Kume, and M. Yamada, Super-slow phase transition catalyzed by BHs and the birth of baby BHs, Phys. Lett. B **849**, 138465 (2024).
- [74] S. Blasi and A. Mariotti, QCD axion strings or seeds?, SciPost Phys. 18, 016 (2025).
- [75] S. Blasi, R. Jinno, T. Konstandin, H. Rubira, and I. Stomberg, Gravitational waves from defect-driven phase transitions: Domain walls, J. Cosmol. Astropart. Phys. 10 (2023) 051.
- [76] R. Balkin, J. Serra, K. Springmann, S. Stelzl, and A. Weiler, Runaway relaxion from finite density, J. High Energy Phys. 06 (2022) 023.
- [77] J. Casalderrey-Solana, D. Mateos, and M. Sanchez-Garitaonandia, Mega-hertz gravitational waves from neutron star mergers, arXiv:2210.03171.
- [78] R. Balkin, J. Serra, K. Springmann, S. Stelzl, and A. Weiler, Heavy neutron stars from light scalars, J. High Energy Phys. 02 (2025) 141.
- [79] M. Laine, Bubble growth as a detonation, Phys. Rev. D 49, 3847 (1994).
- [80] H. Kurki-Suonio and M. Laine, Supersonic deflagrations in cosmological phase transitions, Phys. Rev. D 51, 5431 (1995).
- [81] M. Laine and K. Rummukainen, What's new with the electroweak phase transition?, Nucl. Phys. B, Proc. Suppl. 73, 180 (1999).
- [82] J. R. Espinosa, T. Konstandin, J. M. No, and G. Servant, Energy budget of cosmological first-order phase transitions, J. Cosmol. Astropart. Phys. 06 (2010) 028.
- [83] The plasma frame is defined as the frame in which the center of the bubble is at rest.

- [84] G. Barni, S. Blasi, and M. Vanvlasselaer, The hydrodynamics of inverse phase transitions, J. Cosmol. Astropart. Phys. 10 (2024) 042.
- [85] Y. Bea, J. Casalderrey-Solana, D. Mateos, and M. Sanchez-Garitaonandia, Hydrodynamics of relativistic superheated bubbles, arXiv:2406.14450.
- [86] D. Cutting, E. Vilhonen, and D. J. Weir, Droplet collapse during strongly supercooled transitions, Phys. Rev. D 106, 103524 (2022).
- [87] M. A. Buen-Abad, J. H. Chang, and A. Hook, Gravitational wave signatures from reheating, Phys. Rev. D 108, 036006 (2023).
- [88] C. Caprini and J. M. No, Supersonic electroweak baryogenesis: Achieving baryogenesis for fast bubble walls, J. Cosmol. Astropart. Phys. 01 (2012) 031.
- [89] J. B. Dent, B. Dutta, and M. Rai, Imprints of early Universe cosmology on gravitational waves, J. High Energy Phys. 03 (2025) 098.
- [90] L. O'Raifeartaigh, Spontaneous symmetry breaking for chiral scalar superfields, Nucl. Phys. B96, 331 (1975).
- [91] A. E. Nelson and N. Seiberg, R symmetry breaking versus supersymmetry breaking, Nucl. Phys. **B416**, 46 (1994).
- [92] K. A. Intriligator, N. Seiberg, and D. Shih, Supersymmetry breaking, R-symmetry breaking and metastable vacua, J. High Energy Phys. 07 (2007) 017.
- [93] N. J. Craig, P. J. Fox, and J. G. Wacker, Reheating metastable o'raifeartaigh models, Phys. Rev. D 75, 085006 (2007).
- [94] A. Katz, On the thermal history of calculable gauge mediation, J. High Energy Phys. 10 (2009) 054.
- [95] See Supplemental Material at http://link.aps.org/supplemental/10.1103/pmf7-vlvc for further details on the derivation of the effective potential and other thermodynamical quantities.
- [96] S. Coleman and E. Weinberg, Radiative corrections as the origin of spontaneous symmetry breaking, Phys. Rev. D 7, 1888 (1973).
- [97] M. Quiros, Finite temperature field theory and phase transitions, in *ICTP Summer School in High-Energy Physics and Cosmology* (1999), 1, pp. 187–259, arXiv: hep-ph/9901312.
- [98] D. Curtin, P. Meade, and H. Ramani, Thermal resummation and phase transitions, Eur. Phys. J. C 78, 787 (2018).
- [99] We remind the reader that the velocities v_{\pm} have to be understood in the front frame, where the bubble wall is at rest.
- [100] F. Giese, T. Konstandin, and J. van de Vis, Modelindependent energy budget of cosmological first-order phase transitions—A sound argument to go beyond the bag model, J. Cosmol. Astropart. Phys. 07 (2020) 057.
- [101] L. Leitao and A. Megevand, Hydrodynamics of phase transition fronts and the speed of sound in the plasma, Nucl. Phys. B891, 159 (2015).
- [102] S. R. Coleman, The fate of the false vacuum. 1. Semiclassical theory, Phys. Rev. D 15, 2929 (1977).16, 1248(E) (1977).
- [103] A. D. Linde, Fate of the false vacuum at finite temperature: Theory and applications, Phys. Lett. 100B, 37 (1981).
- [104] A. D. Linde, Decay of the false vacuum at finite temperature, Nucl. Phys. B216, 421 (1983).B223, 544(E) (1983).

- [105] J. Ellis, M. Lewicki, J. M. No, and V. Vaskonen, Gravitational wave energy budget in strongly supercooled phase transitions, J. Cosmol. Astropart. Phys. 06 (2019) 024.
- [106] A. H. Guth and S. H. H. Tye, Phase transitions and magnetic monopole production in the very early Universe, Phys. Rev. Lett. **44**, 963 (1980).
- [107] K. Enqvist, J. Ignatius, K. Kajantie, and K. Rummukainen, Nucleation and bubble growth in a first order cosmological electroweak phase transition, Phys. Rev. D 45, 3415 (1992).
- [108] The relation $T_{\rm nuc}=T_+$ only holds for detonations and antideflagrations. For the other expansion modes, we still use this as a sensible approximation to identify the relevant v_+ branch.
- [109] Y. Bea, M. Giliberti, D. Mateos, M. Sanchez-Garitaonandia, A. Serantes, and M. Zilhão, Bubble dynamics in a QCD-like phase diagram, arXiv:2412.09588.

- [110] W.-Y. Ai, B. Laurent, and J. van de Vis, Modelindependent bubble wall velocities in local thermal equilibrium, J. Cosmol. Astropart. Phys. 07 (2023) 002.
- [111] W.-Y. Ai, B. Laurent, and J. van de Vis, Bounds on the bubble wall velocity, J. High Energy Phys. 02 (2025) 119.
- [112] W.-Y. Ai, X. Nagels, and M. Vanvlasselaer, Criterion for ultra-fast bubble walls: The impact of hydrodynamic obstruction, J. Cosmol. Astropart. Phys. 03 (2024) 037.
- [113] A spectator field does not change its physical properties, e.g., its mass, during the phase transition.
- [114] F. Giese, T. Konstandin, K. Schmitz, and J. van de Vis, Model-independent energy budget for LISA, J. Cosmol. Astropart. Phys. 01 (2021) 072.
- [115] M. Sanchez-Garitaonandia and J. van de Vis, Prediction of the bubble wall velocity for a large jump in degrees of freedom, Phys. Rev. D 110, 023509 (2024).